Effect of different cation-anion bond strengths on metal—ternary-semiconductor interface formation: $Cu/Hg_{0.75}Cd_{0.25}Te$ and Cu/CdTe

D. J. Friedman, G. P. Carey, I. Lindau, and W. E. Spicer
Stanford Electronics Laboratories, Stanford University, Stanford, California 94305
(Received 6 May 1986)

The effect of the very different Hg—Te and Cd—Te bond strengths in $Hg_{1-x}Cd_xTe$ (MCT) upon interface formation with a noble metal is investigated via a comparative study of the Cu/*n*-type CdTe and Cu/*p*-type MCT ($x=0.25$) interfaces formed in ultrahigh vacuum at room temperature. The interfaces were studied using x-ray and ultraviolet photoelectron spectroscopy and low-energy electron diffraction. For Cu/CdTe there is a limited movement of Cd and Te into the Cu and no detectable migration of Cu into the semiconductor. For Cu/MCT, Hg is lost and there is movement of Cu into MCT as well as a pronounced movement of Cd and Te into the Cu for both the low- and high-coverage regimes. At a coverage of 2.5 monolayers (ML) the Cu intermixes into the top ~ 20 Å of the semiconductor as $\sim 20\%$ of the Hg is depleted from this region, while at high coverages (>100 ML) the near-surface region of the Cu overlayer contains roughly 5% Cd and 35% Te, an order of magnitude more Cd and Te than for Cu/CdTe. The differences in the CdTe and MCT behavior are attributed to the weakness of the Hg—Te bond. For MCT, on deposition of 0.1 ML Cu the bands bend 0.1 eV upwards from the initial pinning position of the surface conduction-band minimum (CBM) at the Fermi level E_F (within 0.1 eV). For Cu/CdTe, deposition of 0.1 ML Cu causes the bands to bend 0.2 eV up from their initial pinning position of E_F 0.3 eV below the CBM.

I. INTRODUCTION

In contrast to the vast body of research utilizing surface science techniques on metal interfaces with elementary and binary compound semiconductors such as Si and GaAs, only recently has similar work been initiated upon the technologically important and fundamentally interesting ternary alloy semiconductor $Hg_{1-x}Cd_xTe$.[1–6] Because the band gap of this alloy spans the range 0–1.5 eV as the composition is varied from $x=0$ to $x=1$, $Hg_{1-x}Cd_xTe$ (MCT) is of great technological importance as an infrared photodetector. Difficulties in applying this material in actual devices arise from the large difference in the Cd—Te and Hg—Te bond strengths, reflected in the much lower heat of formation ΔH_f for HgTe than for CdTe: $\Delta H_f(\mathrm{HgTe})=-7.6$ kcal/mol, while $\Delta H_f(\mathrm{CdTe})=-24.1$ kcal/mol.[7] Experimental[8] and theoretical[9] investigations of the electronic structure of MCT have shown that there is a fundamental connection between the band-gap tunability and the instability of the Hg—Te bond, and that the instability of this bond in HgTe is increased in the alloy by the presence of the Cd.

The instability of the Hg bond has been shown to play a crucial role in the bulk and surface electronic properties of MCT.[8] From the earliest investigation[1] of the behavior of the interface of MCT with a metal (Al), it has been clear that the Hg instability is a determining factor in metal/MCT interface formation when the metal is a reactive one such as Al, with $\Delta H_f(\mathrm{Al_2Te_3})=-76.2$ kcal/mol.[7] For this overlayer metal the reactivity of the interface has been found to result in a depletion of essentially all the Hg to a depth of several tens of Å into the surface even at submonolayer coverages, with the resulting excess of Te migrating into the overlayer.[1,2,6] However, while less reactive interfaces such as Ag/MCT (Refs. 5 and 6) and Au/MCT (Ref. 4) give interface morphologies different than for Al/MCT, with less Hg loss at the semiconductor near-surface region, the presence of Hg in the semiconductor still proves to have a significant effect upon the formation of the interface, as seen by a comparison with the interfaces of the same metals on CdTe. An overview discussion of the role of Hg bonding in metal/MCT interface formation is given in Ref. 10.

In the present paper we give a detailed comparative investigation of the Cu/CdTe and Cu/MCT interfaces in the coverage range of 0.1 monolayers (ML) to hundreds of ML, using photoelectron spectroscopy and low-energy electron diffraction (LEED) to probe the first few atomic layers of the interface under ultrahigh vacuum conditions. Although all the noble metals have fairly low heats of formation with Te, the Cu/MCT interface morphology proves very different from the corresponding interfaces with Au and Ag: The degree of Cd movement into the overlayer is significantly greater for Cu than for Au overlayers,[4] while Ag does not stay localized at the MCT surface but instead diffuses in.[5] Furthermore, since Cu is fairly unreactive with Te, $\Delta H_f(\mathrm{Cu_2Te})=-10.0$ kcal/mol,[7] the MCT interface with Cu is as expected quite different from the interface with Al or the similarly reactive Cr.[3] However, a comparison with Cu/CdTe shows that the Cu/MCT interface is still radically altered by the presence of Hg in the lattice, with enhanced intermixing of the semiconductor and overlayer in the entire range of coverages studied.

II. EXPERIMENTAL

Single-crystal bars of *n*-type CdTe (In-doped to $1\times10^{17}/\mathrm{cm}^3$, bulk band gap 1.5 eV) and *p*-type solid-state

recrystallized $Hg_{0.75}Cd_{0.25}Te$ (bulk band gap 0.22 eV) with cross-sectional areas of 5×5 mm^2 were transferred into a previously baked vacuum chamber and then cleaved in ultrahigh vacuum (base pressure less than 1×10^{-10} torr) to reveal a (110) face. Sequential depositions of metal were evaporated onto the room-temperature surface from a tungsten filament at rates of typically 1–3 Å/min for the lower coverages and 6 Å/min for the high ones; overlayer thickness were monitored with a quartz-crystal microbalance. The amount of metal deposited is given in units of a monolayer (ML) which we define to be the surface density of atoms on the MCT (110) face: For $x=0.25$, 1 ML$=6.77\times10^{14}$ atoms/cm^2 which corresponds to 0.80 Å of metallic Cu. The atomic surface density for CdTe differs from that for $Hg_{0.75}Cd_{0.25}Te$ by 1%, which is negligible for our purposes. The surfaces were studied at each coverage by x-ray and ultraviolet photoelectron spectroscopy (XPS and UPS) respectively, using, respectively, a Mg $K\alpha$ x-ray source ($h\nu=1253.6$ eV) and a helium lamp (He I and He II, $h\nu=21.2$ and 40.8 eV). The photoelectrons were analyzed with a double-pass cylindrical mirror analyzer (CMA) which detects electrons emitted in a polar angle range of $42.3\pm6°$ from the CMA axis. This off-normal detection will decrease the "effective" photoelectron escape depth to 75% of the photoelectron scattering length; since this will introduce only a minor correction to, e.g., the estimates of the overlayer thickness, and since none of the relevant escape lengths are known to within 25% anyway, this correction will be ignored. The interfaces were also characterized by LEED using incident electron energies between 50 and 65 eV and beam currents less than 1 μA. We observed no electron-beam-induced surface disruption for MCT or CdTe, in contrast to the disruption reported for CdTe in Ref. 11.

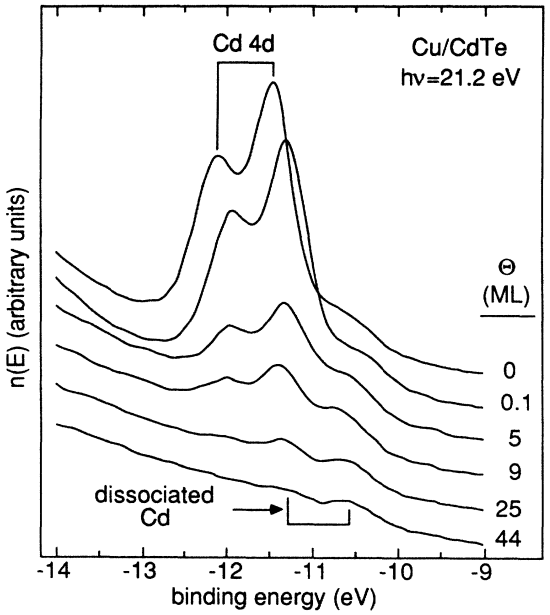

FIG. 1. He I ($h\nu=21.2$ eV) spectra of the Cd 4d shallow core levels with increasing coverage of Cu on CdTe. Energies are referred to the Fermi level.

III. RESULTS: Cu/CdTe

A. Overview

The organization of this section is as follows. In Sec. III B we discuss the initial stages of interface formation, including evidence for Cd dissociation from the semiconductor and for the presence of both reacted and pure metallic Cu. Section III C discusses the intermixing which is observed at high coverages; a more detailed analysis of the high-coverage morphology is given in Sec. III D. More data on interface formation from the LEED observations are presented in Sec. III E, and finally in Sec. III F band bending is briefly discussed.

Figures 1 and 2 show He I ($h\nu=21.2$ eV) spectra of the Cd 4d shallow core level and the valence band as a function of Cu deposition. Between $\Theta=0$ and 0.1 ML all spectral features shift rigidly 0.2 ± 0.05 eV to higher kinetic energy (KE), indicating a bending of the surface bands upwards. For coverages above 2.5 ML, a shifted Cd 4d component emerges at a binding energy 0.8 eV lower than the bulk, and above $\Theta=16$ ML becomes the dominant Cd feature. A shifted Cd peak has previously been observed for Cu/CdTe by Williams *et al.*[12] and is also often observed in other metal/CdTe and related interfaces; the peak originates from Cd dissociated from the semiconductor.[13] In the present case the binding energy (BE) of the shifted Cd $4d_{5/2}$ peak is -10.6 eV, equal to the binding energy of metallic Cd.[14] A calculation[15] of the binding energy expected for Cd dissolved at infinite dilution in Cu gives a shift from the metallic binding energy of only 0.03 eV to higher BE, so that the binding energy of the dissociated Cd, while equal to that of pure metallic Cd, is also consistent with Cd dissolved in the overlayer. Indeed, the

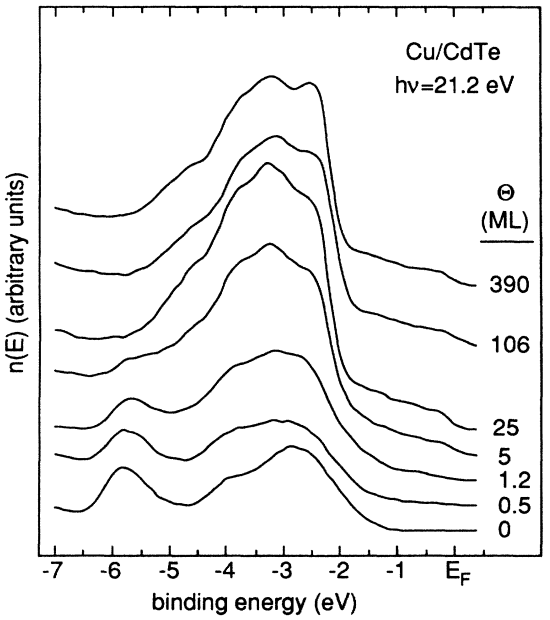

FIG. 2. He I ($h\nu=21.2$ eV) spectra of the valence band with increasing coverage of Cu on CdTe.

slow attenuation of the dissociated Cd $4d$ peak intensity at high coverages implies that the dissociated Cd is in fact mixed with the Cu overlayer.

The evolution of the top of the valence band including the Cu $3d$ states is shown in Fig. 2. The shape of the Cu $3d$ emission changes with coverage, showing a shoulder to high kinetic energy ($\sim$2.5 eV binding energy), which gradually increases in intensity relative to the lower kinetic energy contribution as the Cu coverage increases. A comparison with a reference spectrum of metallic Cu from the literature[16] permits an assignment of the high kinetic energy component of the Cu $3d$, which is clearly visible by $\Theta=5$ ML, to unreacted metallic Cu in the overlayer; the higher binding energy component of the Cu $3d$ line shape must then be due to reacted Cu. It can be seen from Fig. 2 that while the ratio of unreacted to reacted Cu increases with increasing Cu coverage, there is still a significant presence of reacted Cu near the surface of the overlayer even at 390 ML (the highest coverage studied).

B. Initial stages of interface formation: $\Theta < 10$ ML

More detailed information on the nature of the adsorbed Cu at low coverages and the location of the reacted layer at high coverages can be obtained from spectra of the Cu $3d$ states taken with $h\nu=40.8$ eV: At this photon energy the cross sections of the Cd and Te s- and p-derived valence states are negligible, permitting observation of the Cu $3d$ at low coverages, while the greater surface sensitivity to Cu $3d$ with $h\nu=40.8$ eV than 21.2 eV permits an identification of the surface specie. The evolution of the Cu $3d$ states with coverage at $h\nu=40.8$ eV is shown in Fig. 3(a). For the 0.1 and 1.2 ML coverages the semiconductor valence-band contribution has been removed by subtracting the $\Theta=0$ ML spectrum (shifted to account for the band bending, discussed in Sec. III F) from the $\Theta=0.1$ and 1.2 ML spectra; it should be noted that even for $\Theta=0.1$ ML the Cu $3d$ is clearly visible in the unsubtracted spectrum. For the lowest coverage, the low intensity of the Cu $3d$ emission results in a fairly high signal-to-noise ratio in the spectrum. For this reason, along with the data points are shown smooth curves for which the high-frequency noise components have been numerically filtered out. From the figure it can be seen that at $\Theta=0.1$ ML the Cu $3d$ emission is at $\sim$1 eV higher binding energy than for pure metallic Cu, consistent with either Cu adsorption as a reacted Cu-Te phase or with formation of Cu clusters on the surface, which would also lead to a higher Cu $3d$ binding energy than for the bulk metal.[17]

Although at low coverages there should be Te reacted with Cu, and Te bound in the semiconductor, present within an XPS escape length of the surface, the core Te $3d_{5/2}$ state does not show a two-peaked signature of reacted and substrate Te. This absence is in part due to the limited energy resolution for XPS with unmonochromatized Mg $K\alpha$ light, but also suggests that the reacted peak has a binding energy very close to the binding energy for Te in CdTe. The implications of this point will be discussed in Sec. III D. Nonetheless, spectroscopic evidence for reacted Te is available in the width of the XPS core

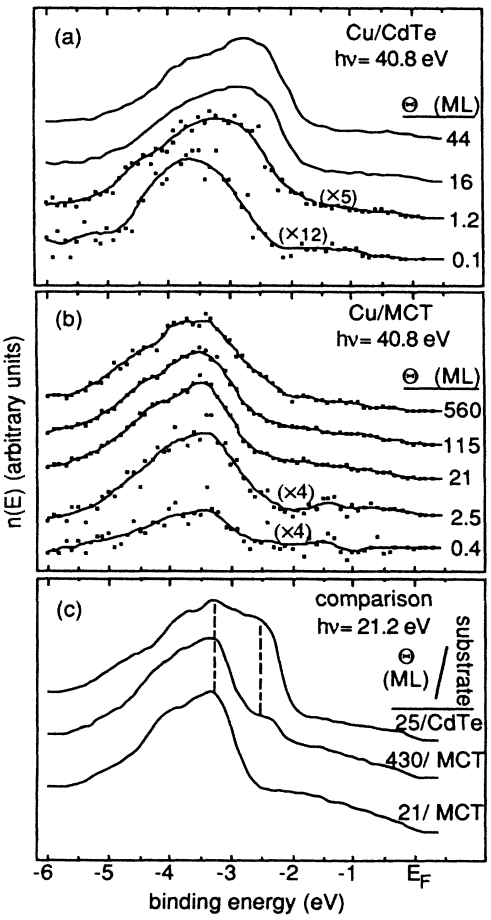

FIG. 3. Evolution of the Cu $3d$ states at $h\nu=40.8$ eV with coverage for (a) Cu/CdTe and (b) Cu/MCT. For $\Theta \leq 2.5$ ML the semiconductor valence-band contribution has been removed by subtracting the $\Theta=0$ ML spectrum (shifted to account for the band bending) from the spectra. The smooth curves through the data points are generated by numerically filtering out the high-frequency noise components. (c) Comparison of the Cu $3d$ emission at $h\nu=21.2$ eV for $\Theta=21$ and 430 ML on MCT, and $\Theta=25$ ML on CdTe, all normalized to equal height.

states, an increase in which can be seen even when two peaks are not explicitly resolvable. Figure 4 shows the evolution of the XPS Te $3d$ and Cu $2p$ core-level widths with Cu coverage. The Te $3d$ width rises to 125% of its zero-coverage value (corresponding to an 0.2 eV increase in FWHM) by $\Theta=10$ ML, as a reacted Te specie forms. The Te width never drops back to its zero-coverage value, indicating that Te occupies several types of inequivalent sites in the reacted layer, as might be expected. For the Cu $2p$, the width rises slightly between $\Theta=0.1$ to 0.5 ML and then starts to fall, paralleling the development of the Cu $3d$ in Fig. 3(a) as the Cu emission evolves from a purely reacted specie to a mixture of reacted and metallic Cu and finally to metallic Cu.

Figure 5 shows on a natural log scale the intensities of the substrate and dissociated Cd $4d$ peak intensities at $h\nu=40.8$ eV. The bulk Cd peak attenuates roughly exponentially with an average escape length of $\sim$7 Å (8.

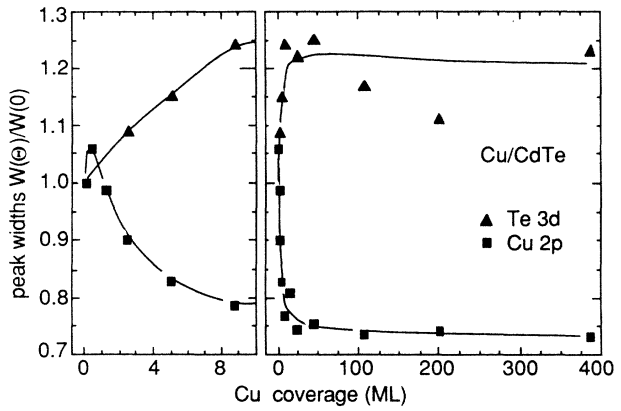

FIG. 4. Variation of the Te $3d$ and Cu $2p$ core widths with coverage for Cu/CdTe.

ML), which is appropriate for attenuation of 25-eV kinetic energy photoelectrons through a laminar overlayer. At coverages below 2.5 ML, however, the bulk Cd peak attenuates somewhat faster, with an equivalent escape length of less than 4 Å. The rapidity of this attenuation rate, which is slightly too fast for simple attenuation through an overlayer, is due to removal of Cd atoms from the semiconductor lattice to form the dissociated specie; correspondingly, the dissociated Cd peak intensity reaches 60% of its maximum value by $\Theta=1.2$ ML and 80% by 2.5 ML.

C. Semiconductor-overlayer intermixing: $\Theta > 10$ ML

The dissociated Cd intensity starts to decrease at $\Theta=25$ ML, suggesting that by this point the formation of Cd in dissociated form is essentially complete. The attenuation rate of the dissociated Cd intensity above $\Theta=25$ ML would correspond to an equivalent exponential attenuation length of ~ 50 Å, much too slow to be consistent with the dissociated Cd forming an abrupt interface with the Cu, and implying instead that the dissociated Cd is intermixed with the Cu overlayer. More quantitatively, the rate of attenuation of the dissociated Cd component above $\Theta=25$ ML is consistent with a fixed amount of Cd being uniformly distributed throughout the overlayer. In this model the concentration of dissociated Cd in the overlayer (and thus also the corresponding photoelectron intensity) would vary inversely with the Cu coverage Θ above $\Theta=25$ ML, at which coverage the formation of dissociated Cd is assumed to have stopped. The attenuation of the dissociated peak given by this model is plotted in Fig. 5 as a dashed line; the match to experiment is quite reasonable.

A comparison of the ratios of metallic to unreacted Cu at $h\nu=21.2$ versus 40.8 eV at high coverages shows that the metallic/reacted ratio is greater for the more surface sensitive 40.8-eV spectra; thus the metallic Cu resides on the surface. Since the surface sensitivity for Cu $3d$ states at $h\nu=40.8$ eV is ~ 7 Å, and reacted Cu can be seen even at this high surface sensitivity, the reacted Cu must lie only a few Å beneath the layer of metallic Cu. Furthermore, the existence of any reacted Cu near the surface of necessity implies the presence of either Cd or Te there for the Cu to react with. The semiconductor specie reacting with the Cu overlayer is more likely to be Te than Cd, considering the greater heat of formation for Cu_2Te than for CuCd: $\Delta H_f(Cu_2Te) = -10.0$ kcal/mol,[7] while $\Delta H_f(CuCd) = -1$ kcal/mol.[18,19]

The presence of a significant quantity of Te in the overlayer is confirmed by Fig. 6, which shows on a natural log scale the attenuation of the XPS peak areas I of the semiconductor with Cu coverage, normalized to the zero-coverage values I_0. Up to $\Theta \approx 16$ ML the Te $3d$ core level (670 eV KE) attenuates exponentially with a decay length of 15 Å, indicative of roughly laminar abrupt coverage. Beyond 16 ML, however, the Te $3d$ attenuation slows so that little attenuation is seen beyond $\Theta \approx 40$ ML; the Te intensity levels off to about 20% of its initial value. Formation of islands of Cu on the surface would also slow the attenuation of the Te $3d$ level below that expected for a laminar interface, but then the Cd and Te intensities would be expected to attenuate at similar rates (Cd 3d: 840 eV KE). Thus while islanding of the Cu is not un-

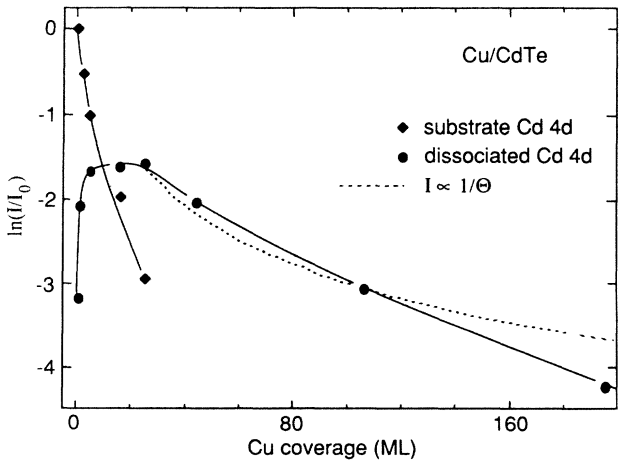

FIG. 5. Attenuation (natural log scale) of the intensities I of the substrate and dissociated Cd $4d$ features at $h\nu=40.8$ eV. The intensities are normalized to the intensity I_0 of the substrate Cd $4d$ peak at zero coverage.

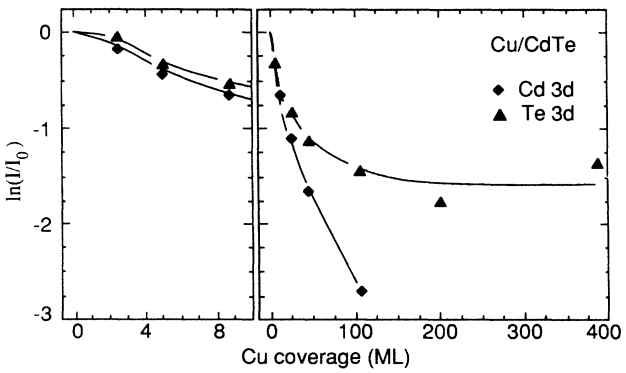

FIG. 6. Attenuation (natural log scale) of the XPS peak areas I of the CdTe core levels with increasing Cu coverage. The peak areas are normalized to their zero-coverage values I_0.

likely, the dependency of I/I_0 on the atom being examined unambiguously indicates intermixing of Te into the overlayer.

The greater intensity of the Te signal compared to the Cd signal at high coverages could indicate a greater quantity of Te intermixed with the overlayer, but might instead simply reflect a different distribution of the Te and Cd atoms in the overlayer, with the Te atoms being concentrated close to the surface instead of being distributed uniformly throughout the overlayer. With Mg $K\alpha$ light, the Te $4d$ falls at 1200 eV KE, making it more bulk sensitive than the Te $3d$ at 670 eV KE; thus a comparison of the Te $3d$ and $4d$ attenuation rates will provide information on the distribution of Te near the surface. Figure 7 shows the intensity ratio $R(\Theta)\equiv I_{\mathrm{Te}\,3d}(\Theta)/I_{\mathrm{Te}\,4d}(\Theta)$ normalized to the zero-coverage value $R(0)$. The observed rise in $R(\Theta)/R(0)$ to ~ 1.5 between $\Theta\approx 16$ and 100 ML thus indicates the development of a Te-rich layer at or near the surface of the overlayer. The coverage at which $R(\Theta)$ starts to rise, $\Theta\approx 16$ ML, coincides with the coverage at which the attenuation of the Te $3d$ intensity slows from its previous exponential laminarlike rate. Thus above roughly this coverage Te starts being pulled into the overlayer, leaving an increasingly thick layer of Cu between the intermixed Te layer and the bulk of the semiconductor. By $\Theta=100$ ML the Te subsurface layer is fully formed and the thickness of the Cu underneath it is sufficiently greater than a Te $4d$ escape length ($\sim$25–30 Å) that $R(\Theta)$ levels off.

By $\Theta=25$ ML the Cu $2p$ width has stabilized at a value equal (within 3%) to the width of metallic Cu as determined from a Cu/stainless steel reference. While greater shifts would be expected for valence Cu $3d$ states than for core Cu $2p$ states upon interaction with Te, the Cu $3d$'s are sufficiently corelike that we would not expect the corresponding Cu $2p$ shift to be as much as an order of magnitude smaller. Therefore the inability of the XPS Cu $2p$ width to reflect the presence of reacted Cu near the surface as seen in UPS cannot be fully explained by the relatively poorer energy resolution in XPS, as the energy difference between the reacted and metallic Cu $3d$ positions is seen from Figs. 2 and 3(a) to be about 0.8 eV. Instead, the absence of a reacted Cu signature in the Cu $2p$ at high coverages must be due to the longer escape length for XPS Cu $2p$ than for UPS Cu $3d$, indicating that the reacted Te layer is significantly thinner than an XPS Cu $2p$ escape length of order 10 Å. The thickness and location of the Te-containing subsurface layer will be discussed in more detail in Sec. III D.

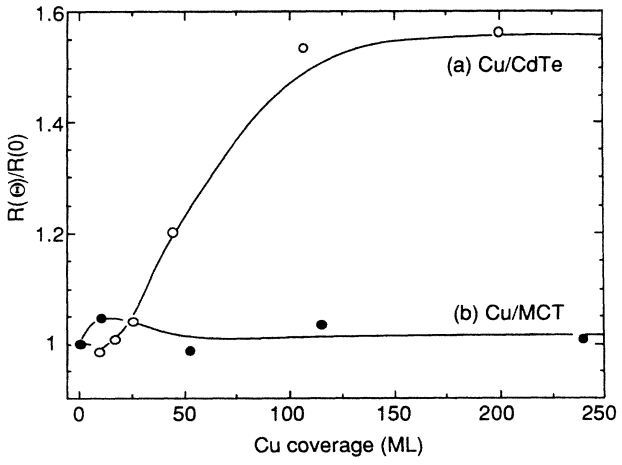

FIG. 7. Intensity ratio $R(\Theta)\equiv I_{\mathrm{Te}\,3d}(\Theta)/I_{\mathrm{Te}\,4d}(\Theta)$ normalized to the zero-coverage value $R(0)$, for (a) Cu/CdTe and (b) Cu/MCT.

D. Escape depth analysis

Thus far only a qualitative analysis of the interface morphology at high coverages has been given. However, given reasonable assumptions about the variation of electron escape depth with kinetic energy, the interface can be analyzed in a more quantitative way using $R(\Theta)$ from Fig. 7 and the Te $3d$ attenuation from Fig. 6. In this section we attempt to quantify the previous discussion of the location and thickness of the subsurface Te-rich layer for high Cu coverages Θ by introducing an idealization of the previous description of this layer. The formation of the Te layer appears to be complete above $\Theta=100$ ML, with the Te $3d$ intensity as well as $R(\Theta)$ being essentially constant above this coverage. For concreteness we shall analyze the interface at $\Theta=390$ ML.

Specifically, we model the concentration of Te in the thick Cu overlayer as being uniform between depths d and $d+\Delta$ from the surface and zero elsewhere, so that Δ is the thickness of the layer. We denote the XPS escape lengths of Te $3d$ and Te $4d$ photoelectrons in the overlayer by λ_1 and λ_2, respectively, the corresponding escape lengths in the semiconductor by λ_1^S and λ_2^S, and define $A=\lambda_1/\lambda_2$. The presence of the Te layer in the Cu is assumed not to affect the electron escape lengths significantly. Let $I_1/I_1(0)$ and $I_2/I_2(0)$ be, respectively, the Te $3d$ and Te $4d$ intensities at $\Theta=390$ ML, normalized to their respective intensities at $\Theta=0$. Finally, we denote the Te concentration (i.e., number of atoms per unit volume) in the layer to be K times the Te concentration in the bulk. K is a dimensionless number, the magnitude of which is estimated in the Appendix.

The photoelectron intensity from a subshell of atom A with quantum numbers n,l excited by photons $h\nu$ to kinetic energy E depends on the concentration $c(x)$ of atoms A at distance x from the surface and the electron escape length $\lambda(E)$ by

$$I=T(E)\sigma_{nl}(E,h\nu)F(E)\int_0^\infty e^{-x/\lambda(E)}c(x)dx\ . \qquad (1)$$

Here $T(E)$ is the theoretical CMA transmission; σ_{nl} is the subshell partial photoionization cross section (PPCS), and F includes all other effects. The Mg $K\alpha$ light excites the core levels of interest to sufficiently high kinetic energies that the energy dependence[20] of F is negligible for our purposes.

Details of the escape length calculation and estimates of the parameters are given in the Appendix. A plot of d/λ_1 versus Δ/λ_1 from Eqs. (A2) and (A3) for the range of parameters discussed in the Appendix is shown in Fig. 8. The allowed values of d/λ_1 and Δ/λ_1 lie in the shaded region. Taking $\lambda_1\approx 15$ Å, the figure indicates a minimum

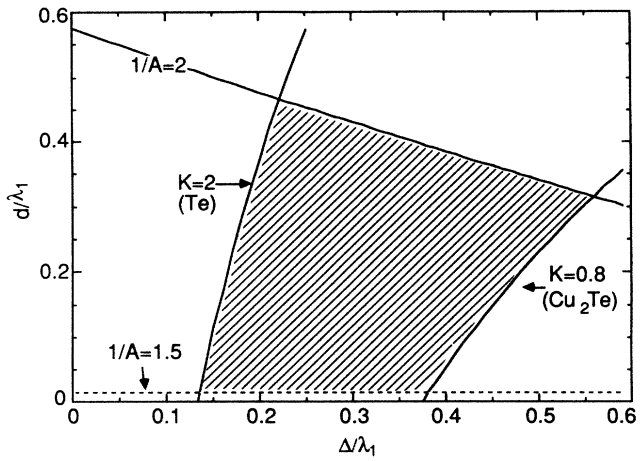

FIG. 8. Plot of d/λ_1 vs Δ/λ_1 from Eqs. (A2) and (A3) for the Te subsurface layer model for Cu/CdTe. The values of d/λ_1 and Δ/λ_1 corresponding to the most likely values of the parameters A and K lie in the shaded region.

layer thickness of 2 Å at the maximum allowed Te density, and a maximum thickness of 8 Å at the minimum density. The layer lies at most 7 Å beneath the surface. Although these numbers are certainly not exact, they should provide a reliable estimate of the order of magnitude of the depth and thickness of the Te-containing layer. The values provide an explanation of the absence of any reacted-Cu signature in the XPS Cu $2p$: The layer is thin and lies close to the surface, contributing less to the XPS spectra than to the more surface-sensitive UPS spectra. A layer extending even moderately far below the surface is allowed only for low values of the Te concentration, implying a correspondingly less intense reacted Cu component to which the XPS would be less sensitive than the UPS.

For every Te atom pulled from the semiconductor lattice into the overlayer an average of one Cd atom will also be freed from the lattice. If there were significantly more Te than Cd intermixed into the overlayer, there would be a resulting excess of Cd remaining at the semiconductor surface; i.e., localized between the MCT and the overlayer. This excess Cd would contribute to the shifted Cd $4d$ peak and at low coverages would be the dominant contribution to this peak. However, as more Cu was deposited on the surface this dominant contribution from the localized Cd would attenuate with the appropriate laminarlike escape length of ~ 7 Å. The fact that the shifted Cd peak does not attenuate in this fashion, as evident in Fig. 5, suggests that the amount of Te and Cd intermixed into the overlayer might be comparable, and that the differences in the intensities of the intermixed Cu $3d$ and Te $3d$ at high coverages is due to the different distribution of Cd and Te in the overlayer. It is thus of interest to estimate the relative amounts of Te and Cd in the high-coverage Cu overlayer on the basis of our model of uniform distribution of the Cd and layer distribution of the Te. The total amount of Cd in the overlayer for $\Theta \geq 25$ ML is assumed to be equal to the amount at $\Theta = 25$ ML, and to be distributed uniformly throughout the overlayer. From Fig. 5, the intensity the shifted Cd $4d$ signal at this coverage is 18% of the Cd $4d$ signal for cleaved CdTe. Thus (neglecting the variation in escape length with material which will not change the answer significantly) the number of Cd atoms $N_{\mathrm{Cd:Cu}}$ in the Cu per unit surface area of the sample is $N_{\mathrm{Cd:Cu}} = 0.18 \times (20\text{Å}) \times N_{\mathrm{Cd:CdTe}}$, where $N_{\mathrm{Cd:CdTe}}$ is the number of Cd atoms per unit volume in CdTe ($N_{\mathrm{Cd:CdTe}} = N_{\mathrm{Te:CdTe}}$). The number of Te atoms per unit area in the subsurface layer is just $N_{\mathrm{Te:Cu}} = \Delta \times K \times N_{\mathrm{Te:CdTe}}$, the range of allowed values for which can be read off from Fig. 8. We find that $N_{\mathrm{Cd:Cu}}/N_{\mathrm{Te:Cu}} \approx 0.5-1$; that is, the model yields a comparable total amount of Cd and Te in the Cu overlayer.

This result for $N_{\mathrm{Cd:Cu}}/N_{\mathrm{Te:Cu}}$ should not necessarily be taken literally, because it depends sensitively upon an assumption that there is no Te elsewhere in the overlayer than in the subsurface layer. While the subsurface layer must dominate Te emission from the overlayer, a low concentration of Te distributed throughout the overlayer in addition to the Te in the subsurface layer would not be inconsistent with the data (nor would it invalidate the estimate of the depth and thickness of the layer). Thus $N_{\mathrm{Cd:Cu}}/N_{\mathrm{Te:Cu}}$ might actually be significantly less than 0.5. However, this estimate for $N_{\mathrm{Cd:Cu}}/N_{\mathrm{Te:Cu}}$ is consistent with the absence of evidence for dissociated Cd localized at the semiconductor surface. More importantly, the result illustrates a general danger in concluding from core-level intensity plots (such as Fig. 6) alone that different semiconductor components have significantly different degrees of intermixing with the overlayer.

E. LEED observations

Further information on the morphology of the interface is provided by the LEED observations of the surface. The primary-beam current of 50–65 eV used for the LEED observations provides a very high surface sensitivity, to at most the first two or three atomic layers. The initially sharp 1×1 LEED pattern becomes slightly more diffuse upon the initial deposition of 0.1 ML Cu, but still remains fairly sharp up to $\Theta = 2.5$ ML. Between $\Theta = 2.5$ and 5 ML the pattern becomes significantly more diffuse, finally disappearing beyond $\Theta \approx 25$ ML. These observations are consistent with incomplete coverage of the surface up to 2.5-ML coverage, permitting diffraction from the uncovered areas of the CdTe; alternatively the Cu could be forming an ordered overlayer at low coverage. By $\Theta = 5$ ML microcrystallites of Cu_xTe or Cu with size on the order of a LEED coherence length have formed, giving rise to the diffuse pattern seen at this and higher coverages. The lack of any sharp spot contributions to the observed pattern at and above $\Theta = 5$ ML suggests that the CdTe is completely covered by the overlayer by this coverage. Above 25 ML the surface is disordered. It is interesting to note that Ehsani and Bené,[21] using transmission electron microscopy and diffraction on 200 Å Cu thick overlayers deposited on CdTe at 3×10^{-7} torr, have observed crystalline Cu as well as Cu_2Te crystallites.

F. Schottky-barrier formation

The Fermi-level position for the cleaned cleaved n-CdTe surface was found to lie $03. \pm 0.1$ eV below the

conduction-band minimum (CBM), representing a pinning of E_F below the position for the bulk n-type CdTe (a number of clean cleaved surfaces were studied, and this pinning position within 0.1 eV was observed in all cases). The band bending, visible in Fig. 1 and complete by the initial 0.1-ML coverage, shifts E_F about 0.2 eV further down from the CBM, giving a Schottky-barrier height of roughly 0.5 eV. This value compares favorably with Patterson and Williams's value[12] of 0.45 eV measured by I-V.

IV. RESULTS: Cu/MCT

A. Overview

Section IV is organized much like Sec. III which presented the Cu/CdTe results. The low-and high-coverage regimes are presented in Sec. IV B and IV C, respectively; Sec. IV D discusses the LEED observations, and Sec. IV E discusses band bending.

Figure 9 shows He I spectra of the Hg $5d$ and Cd $4d$ shallow core levels as Cu is deposited on the surface. For the cleaved surface the Fermi level E_F is located within ± 0.1 eV of the conduction-band minimum (CBM) making the surface intrinsic or n type (even though the sample is bulk p type), as is often observed.[22] A rigid shift of all spectral features 0.1 eV to higher kinetic energy, due to band bending, occurs upon deposition of the initial 0.1-ML coverage; the band bending appears to have stabilized by this coverage. The Hg $5d$ peaks, the dominant feature for the cleaved surface, attenuate rapidly upon Cu deposition, with $I/I_0 \approx 10\%$ by $\Theta = 10$ ML. The rapidity of this attenuation suggests that Hg is being depleted from the surface. (A detailed examination of this possibility will be given in Sec. IV B.) In contrast, the Cd $4d$ feature is visible even at coverages beyond 100 ML, indicating the presence of Cd in the overlayer. However, in contrast to the binding energy of the intermixed Cd $4d_{5/2}$ peak for Cu/CdTe which appeared at the pure metallic Cd binding energy of -10.6 eV, the intermixed Cd $4d_{5/2}$ peak for MCT appears at about 0.2 eV higher binding energy. Therefore this intermixed Cd can be neither segregated in the form of pure Cd metal nor simply alloyed with Cu, as was the case for CdTe; another element, Te, must also be present in sufficient quantities to affect the Cd $4d$ binding energy.

The evolution of the Cu $3d$ states at $h\nu = 21.2$ eV, pictured in Fig. 10, also differs from the case of CdTe. At coverages up to 115 ML, only one contribution to the Cu $3d$ emission is present; it falls at the same binding energy as the reacted Cu $3d$ contribution for CdTe. By the 365 ML coverage, a shoulder appears at the high kinetic energy side of the reacted Cu $3d$ feature, at a binding energy corresponding to unreacted Cu. With increasing coverage the intensity of this component grows, but even at $\Theta = 560$ ML (the highest coverage studied) the reacted-Cu component still dominates the Cu $3d$ emission. The identification of the correspondence of the reacted and unreacted Cu $3d$ features between MCT and CdTe is supported by Fig. 3(c), which compares He I spectra of the Cu $3d$ emission for $\Theta = 21$ and 430 ML on MCT, and $\Theta = 25$ ML on CdTe. It can be seen that the unreacted and reacted Cu $3d$ binding energies are the same for the MCT and CdTe spectra, while the ratios of the two contributions are very different. For the 21 ML on MCT spectrum, there is no unreacted Cu present.

As with Cu/CdTe, examination of the Cu $3d$ peaks at $h\nu = 40.8$ eV provides further information on the nature of the adsorbed Cu at low coverages and the overlayer morphology at high coverages. He II spectra of the Cu $3d$ are shown in Fig. 3(b). For $\Theta \lesssim 2.5$ ML the semiconduc-

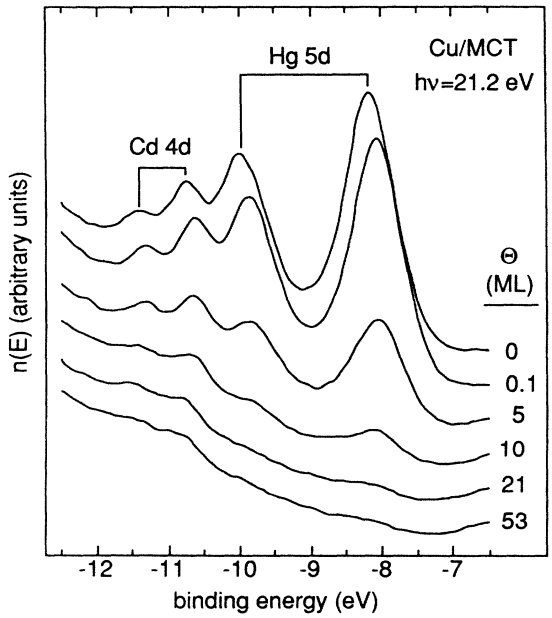

FIG. 9. He I spectra of the Cd $4d$ and Hg $5d$ shallow core levels with increasing coverage of Cu on MCT. Energies are referred to the Fermi level.

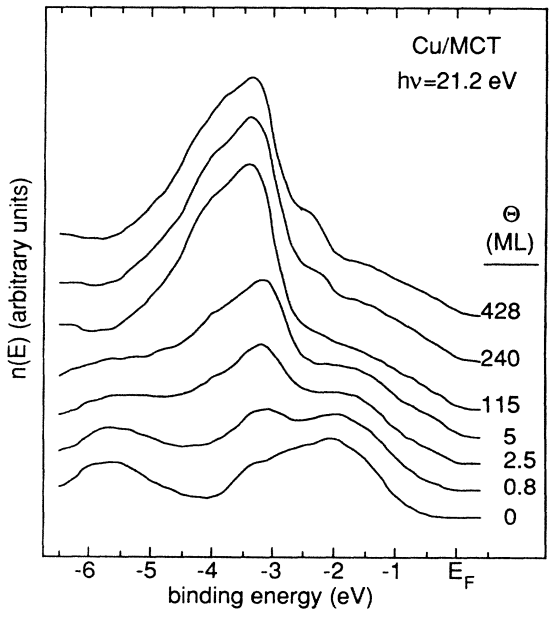

FIG. 10. He I spectra of the valence band with increasing coverage of Cu on MCT.

tor valence-band contribution has been removed by subtracting the $\Theta=0$ ML spectrum (shifted to account for the band bending) from the Cu/MCT spectra. The Cu $3d$ from the initially adsorbed Cu appears at the reacted-Cu binding energy; this binding energy position is stable with coverage. The stability of the Cu $3d$ line shape and binding energy from the lowest coverages to coverages much greater than one ML, for which size effects on the binding energy due to clustering will play no role, suggests that the initially deposited Cu is adsorbed in reacted form. A comparison of the $h\nu=21.2$ and 40.8 eV spectra at coverages of 240 ML and above, for which the unreacted-Cu component is present, show no significant differences in the observed ratio of unreacted to reacted Cu $3d$. This similarity between the two spectra with different surface sensitivities suggests that the unreacted metal is covering the reacted phase by island formation rather than laminarly.

B. Morphology at low coverages: $\Theta<3$ ML

A comparison of the low-coverage valence-band spectra for CdTe (Fig. 2) to those for MCT (Fig. 10) shows a smaller Cu $3d$ intensity (both reacted and unreacted) for MCT than for CdTe at comparable coverages. This observation is supported by Fig. 11, which compares the XPS peak area ratio $R_{\mathrm{Cu}}=I_{\mathrm{Cu}\,2p}(\Theta)/I_{\mathrm{Te}\,3d}(0)$ for MCT and CdTe. Since the initial Te concentration is the same for MCT and CdTe, and since variations in photon flux and experimental geometry cancel in this ratio, the ratio can be directly compared for the two interfaces. At high coverages, $R_{\mathrm{Cu}}(\mathrm{MCT})\approx 0.7\times R_{\mathrm{Cu}}(\mathrm{CdTe})$, simply reflecting the fact that at high coverages the composition of the overlayer near surface is only $\sim$60–70% Cu for MCT and almost 100% Cu for CdTe. More significantly, $R_{\mathrm{Cu}}(\mathrm{MCT})$ is also on the order of half of $R_{\mathrm{Cu}}(\mathrm{CdTe})$ at low coverages. At $\Theta=2.5$ ML, for example, $R_{\mathrm{Cu}}(\mathrm{MCT})\approx 0.5\times R_{\mathrm{Cu}}(\mathrm{CdTe})$. This disparity could be explained as indicating either a smaller amount of Cu stuck to the MCT at the same nominal coverage due to a lower sticking coefficient on MCT or experimental error in the calibration of the coverages, or motion of the adsorbed Cu sufficiently deep into the MCT to attenuate the Cu signal by a factor of 2 compared to the CdTe case. For the former explanation, a factor of 2 difference in sticking coefficient between CdTe and MCT seems unlikely, especially as there is no obvious reason why the sticking coefficient should be significantly less than one in either case. Although there is undoubtedly some error in the calibration of the coverages, the depositions were done carefully in a consistent manner for CdTe and MCT, so that at $\Theta=2.5$ ML the ratio of the actual coverages for equal nominal coverage is estimated to be well within a factor of 1.5 at worst. The consistency with which $R_{\mathrm{Cu}}(\mathrm{MCT})\approx 0.5 R_{\mathrm{Cu}}(\mathrm{CdTe})$ for all low coverages also tends to rule out the explanation of calibration error.

Therefore the disparity in intensity of the Cu intensities from Cu/CdTe and Cu/MCT at low coverages implies that the Cu moves into the MCT instead of being localized upon the surface. Although a significant motion of the overlayer metal at room temperature is not seen for

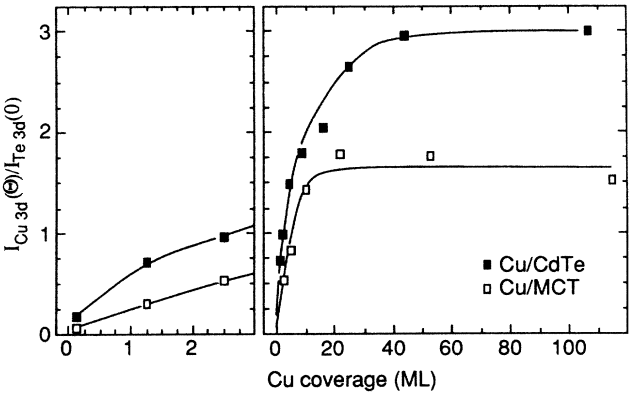

FIG. 11. Core-level intensity ratio $I_{\mathrm{Cu}\,3d}(\Theta)/I_{\mathrm{Te}\,3d}(0)$ for Cu/CdTe and Cu/MCT.

such semiconductors as Si or GaAs, one would expect MCT to behave differently, and indeed Ag moves 10^2–10^3 Å into the MCT surface at room temperature.[5] To estimate the extent of the "in-diffusion" of Cu into the MCT at low coverages we again invoke escape depth arguments based on Eq. (1). Consider for concreteness the 0.8 ML coverage, and suppose that the Cu moves into the MCT to give a concentration $c(x)$ at depth x from the surface which is a constant C at depths less than d from the surface, and zero for $x>d$. [The exact form for the intermixing $c(x)$ is unimportant; any reasonable form for $c(x)$ will yield a similar estimate for the intermixing depth.] By assumption the same number of Cu atoms N per sample surface area is deposited on CdTe and MCT, so that for MCT we have $N=d\times C$. For CdTe at low coverage the Cu atoms reside on the CdTe surface and photoelectrons can escape from each atom to the vacuum without being attenuated by any overlying atoms. Denote this unattenuated photoelectron intensity per Cu atom by I_{atom}, so that the total Cu intensity per unit area from CdTe is $I_{\mathrm{Cu:CdTe}}=NI_{\mathrm{atom}}$. For the case of Cu in MCT, the photoelectron intensity from Cu atoms at depth x will be attenuated according to Eq. (1), so that $I_{\mathrm{Cu:MCT}}=C\lambda(1-e^{-d/\lambda})$. Then since $R_{\mathrm{Cu}}(\mathrm{MCT})/R_{\mathrm{Cu}}(\mathrm{CdTe})=I_{\mathrm{Cu:CdTe}}/I_{\mathrm{Cu:CdTe}}$ we obtain finally

$$(1-e^{-d/\lambda})(\lambda/d)=R_{\mathrm{Cu}}(\mathrm{MCT})/R_{\mathrm{Cu}}(\mathrm{CdTe})\approx 0.4 \text{ at } \Theta=0.8 \text{ ML},$$

which gives $d=2.2\lambda\approx 25$–35 Å as the depth to which Cu moves into the MCT at low coverages. As a consistency check, a calculation from the XPS core-level intensities of the concentration of Cu in the MCT near-surface region at $\Theta=0.8$ ML assuming a uniform distribution gives a concentration of 10% Cu. The amount of Cu in a 0.7 ML coverage can be distributed as 10% of an atomic layer for 7 layers or 16 Å into the bulk, within a factor of 2 of the estimate of d. Similar results are obtained at other (low) coverage values.

The attenuation rates of Hg $5d$ and Cd $4d$ levels at $h\nu=40.8$ eV are shown in Fig. 12. Below $\Theta=2.5$ ML ($=2$ Å) both levels attenuate with a $1/e$ length of about 3 Å.[23] Even if the interface were abrupt and laminar,

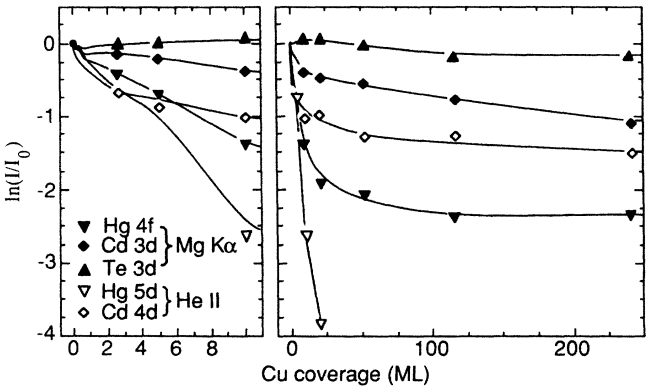

FIG. 12. Attenuation (natural log scale) of the peak areas I of the MCT core levels with increasing Cu coverage. The peak areas are normalized to their zero-coverage values I_0.

with all the Cu staying on the surface to provide the maximum attenuation of the semiconductor signal intensities, this attenuation would be somewhat faster than the expected escape length of 5–7 Å, implying that the first few Å of the semiconductor nearest the interface are deficient in Cd and Hg. In fact, as noted above, at low coverages the Cu does not reside on the surface of the semiconductor but intermixes to a depth on the order of 20 Å. Thus a Hg and Cd deficient Te-rich surface layer of 3–4 Å at $\Theta=2.5$ ML would be required to provide the observed attenuation of the Hg and Cd intensities. The attenuation of the Cd $3d$ core level at a rate consistent with virtually laminar coverage, and the leveling off of the Cd $4d$ intensity beyond $\Theta=2.5$ ML, imply that the Cd deficiency is confined to within a few Å of the interface.

In the case of Hg, however, the rapid attenuation of the Hg $4f$ intensity and the continued rapid attenuation of the Hg $5d$ intensity up to $\Theta=10$ ML suggest a Hg depletion extending beyond the Cd deficient layer localized at the interface. At coverages up to 10 ML, the Hg $4f$ attenuates with a $1/e$ length of less than 6 Å. Since the photoelectron escape length for Hg $4f$ electrons with Mg $K\alpha$ light is ~20–25 Å, at $\Theta=2.5$ ML this attenuation rate implies a Hg depletion in more than just the 3–4 Å surface layer. The attenuation of the Hg $5d$ and $4f$ intensities at $\Theta=2.5$ ML can be reconciled by attributing the "extra" Hg depletion implied by the Hg $4f$ attenuation to an additional depletion of ~20% of the Hg in the ~20 Å beneath the ~3–4 Å layer which is completely depleted of Hg and Cd. The continued rapid Hg $4f$ depletion up to $\Theta=10$ ML and subsequent leveling off implies a continued loss of Hg up to this coverage. For Hg $4f$ at $\Theta=10$ ML ($=8$ Å), $I/I_0\approx 25\%$. Even if the Cu were forming a laminar 8 Å thick overlayer at this coverage, attenuation through this overlayer and the 3–4 Å thick layer which is completely Hg and Cd depleted would only result in $I/I_0\approx 50$–65%, implying a further depletion of ~50–60% of the Hg in the next 20 Å.

From Eq. (1), for a fixed experimental geometry and photon flux the concentrations c_1 and c_2 of atoms 1 and 2 in a sample of uniform composition will be related to the XPS peak areas I_1 and I_2 by $c_2/c_1=(S_2/S_1)(I_2/I_1)$, where $S\equiv[\lambda(E)T(E)\sigma(E)]^{-1}$ is the atomic sensitivity. Although the composition of the Cu/MCT near-surface region at low coverages is not homogeneous, a calculation of the percent composition of each component using the atomic sensitivity factors will have meaning as an average of the composition over an XPS escape length of 20–30 Å. Also, since the Cu is intermixed into the semiconductor to a depth of this magnitude, such a calculation will provide a more accurate treatment of the Cu concentration than if the Cu were localized on the surface. For this purpose, knowledge of the partial photoionization cross sections (PPCS), as well as the energy dependence of the analyzer transmission $T(E)$ and the escape lengths $\lambda(E)$, are required. We use the calculated PPCS from Ref. 24, making the often used[25] approximation $\lambda(E)=\text{const}\times E^{3/4}$ in the absence of experimental data on this parameter for Cu-Te alloys or for Cu at the required kinetic energies, and take the theoretical transmission $T(E)=\text{const}/E$ at constant pass energy. From zero coverage to $\Theta=0.8$ ML the average composition of the near surface as estimated with the atomic sensitivities changes so that the reduction of the concentrations of the semiconductor components compared to zero coverage becomes 82% for Hg, 90% for Cd, and 96% for Te. The Cu concentration at this coverage is calculated as 10%. Thus while the decrease in Te concentration can be attributed to dilution from the intermixed Cu, both Cd and Hg show a greater decrease due to migration of these cations away from the surface. The decrease in Cd concentration is consistent with complete Cd depletion from the first monolayer, as estimated above. The Hg concentration at $\Theta=0.8$ ML indicates much greater Hg depletion than for Cd, consistent with removal of 20% of the Hg in the first 20 Å or a greater degree of depletion to a smaller depth.

In comparison to the Cu/CdTe case, for which a metallic Fermi edge is visible by 1 ML, for Cu/MCT a clear Fermi edge is not present until 5–10 ML coverage, consistent with the much greater Cu indiffusion and interface intermixing observed for Cu/MCT at low coverages.

C. Semiconductor-overlayer intermixing: $\Theta>3$ ML

The presence of significant quantities of Te in the overlayer at high coverages, suggested by the dominance of reacted Cu $3d$ in the valence-band spectra, is confirmed by Fig. 12, which shows on a natural log scale the attenuation of the peak areas I of the MCT with Cu coverage, normalized to the zero-coverage values I_0. For the Te $3d$ core level, beyond $\Theta=100$ ML I/I_0 virtually levels off at 80–85%, maintaining this intensity even at coverages of several hundred Å. This value for I/I_0 reflects a much greater Te intermixing for MCT than for CdTe, which is in turn responsible for the much larger percentage of Cu being in reacted form for MCT than for CdTe. The complete absence of any unreacted Cu $3d$ signal at coverages up to 100 ML implies a concentration of intermixed Te high enough to react with all the Cu present in the overlayer, from the surface to a depth of at least the problem depth for Cu $3d$ at $h\nu=21.2$ eV (kinetic energy 13 eV), on the order of 10–20 Å. Furthermore, the ratio of Te core-level intensities at different escape depths

$R(\Theta) \equiv I_{\mathrm{Te}\,3d}(\Theta)/I_{\mathrm{Te}\,4d}(\Theta)$, shown in Fig. 7, is virtually constant up to $\Theta = 300$ ML, suggesting a fairly uniform distribution of Te in the overlayer rather than a surface or subsurface layer segregation as seen for CdTe. However, there is admittedly no direct spectroscopic evidence that the composition of the overlayer is uniform at depths significantly deeper than an XPS escape length.

The Cd $3d$ peak intensity attenuates with an equivalent escape length of ~ 20 Å up to $\Theta = 10$ ML, indicating limited Cd intermixing below this coverage. At higher coverages, the attenuation slows so that $I/I_0 \approx 30\%$ at $\Theta = 430$ ML. While some islanding of the Cu may be occurring at lower coverages, the large value of I/I_0 at such a high coverage rules out islanding as the cause for the visibility of the Cd at high coverages; the Cd must be truly intermixed with the overlayer. As noted above, however, the 0.2 eV higher Cd $4d$ binding energy than for pure metallic Cd shows that the dissociated Cd is neither in segregated metallic form nor intermixed with Cu alone. Rather, the high and uniform concentration of Te in the overlayer near surface provides an environment for the intermixed Cd which is sufficiently electronegative to make the intermixed Cd binding energy 0.2 eV deeper than for pure metallic Cd. In comparison, for CdTe the Te was localized in a thin layer which could affect only a small fraction of the uniformly distributed Cd.

Below $\Theta = 10$ ML, the Hg $4f$ attenuates with an average equivalent escape length of about 6 Å; as with the Cd and Te core levels, the Hg $4f$ attenuation slows above 10 ML coverage, so that at $\Theta = 430$ ML $I/I_0 \approx 7\%$ and the attenuation has almost stopped. It seems unlikely that even 7% of the MCT surface could be uncovered at this high a coverage due to islanding; further, if the residual Hg signal were due to islanding, the extremely slow rate of attenuation of the signal with coverage at high coverages would indicate a purely vertical island growth, which also is unlikely. Therefore Hg, as well as Cd and Te, appears to be intermixed into the overlayer at high coverages, although to a much smaller degree. From the He I spectra of Fig. 9 it can be seen that above $\Theta = 53$ ML the Hg $5d$ has attenuated beyond the point of detectability, while the Hg $4f$ is still visible and of almost constant intensity at higher coverages as shown in Fig. 12. Thus while Hg is present in the overlayer even at the highest coverages, as evidenced by the Hg $4f$ emission, the fact that the UPS Hg $5d$ with its shorter escape length is too small to be seen indicates that the Hg is inhomogeneously distributed in the overlayer, with no Hg present within several UPS escape lengths (~ 20 Å) of the surface. The exact reason for this is unclear, but it may reflect the high vapor pressure of Hg combined with the slight instability of Hg at infinite dilution in Cu as measured by the heat of solution of Hg in Cu, $\Delta H_{\mathrm{sol}}(\mathrm{Hg;Cu}) = +0.3$ kcal/mol;[26] in comparison, $\Delta H_{\mathrm{sol}}(\mathrm{Cd;Cu}) = -2$ kcal/mol.[26]

Assuming that the composition of the overlayer is uniform at depths of less than 20 Å (i.e., within the surface layer containing no Hg) this composition can be estimated from the ratios of the XPS peak areas using the atomic sensitivity factors, since the intensities for all components but the Hg will be dominated by the emission from the first 20 Å. The atomic sensitivity factors then yield for the composition of the top 20 Å of the overlayer at $\Theta = 115$ ML (the highest coverage for which only reacted Cu is observed) the rough values 5% Cd, 35% Te, and 60% Cu. A slight extension of the method gives 5% Hg, 5% Cd, 33% Te, and 57% Cu for the composition at deeper than 20 Å. In contrast, an estimation of the average composition of the first ~ 20 Å of the Cu/CdTe near surface at $\Theta = 390$ ML using the atomic sensitivity factors yields a composition of about 7% Te, 0.6% Cd, and 92% Cu. As a reliability check, the composition for the cleaved MCT surface is calculated in the same fasion as 35.4% Hg, 13.4% Cd, and 51.2% Te, which is close to the nominal composition of $Hg_{0.75}Cd_{0.25}Te$. As expected, for Cu/MCT the Te concentration is sufficiently high to provide the Cu and Cd with a Te-rich environment, resulting in the observation of these two components being in "reacted" phases. Both semiconductor cations are present only in residual quantities. It is interesting to note that within the expected error of the estimation of composition, for Cu/MCT the ratio of the Cu and Te concentrations in the near surface is approximately the same as for the stable compound[27] Cu_2Te.

The evolution of the Cu $2p$ and Te $3d$ core widths, reflecting the chemical interaction of these two elements as Cu intermixes with the semiconductor, is shown in Fig. 13. The Te $3d$ core width evolves much as with Cu/CdTe, leveling off by $\Theta = 5$ ML at 120% of its initial value as the Te encounters an increasing concentration of neighboring Cu. The Cu $2p$ core width evolves differently than for Cu/CdTe, rapidly leveling off to 85% of its initial value below $\Theta = 1.2$ ML. Since the Cu is in purely reacted form for all but the highest coverages, the decrease of the Cu $2p$ width from $\Theta = 0.1$ to 1.2 ML must be due to a decreasing number of inequivalent sites for the reacted Cu, reflecting increasing uniformity of the Cu intermixing. In further contrast to Cu/CdTe, and as expected given that the Cu is in reacted form even at high coverages, the Cu $2p$ width for Cu/MCT never decreases to the width measured for the metallic Cu reference spectrum.

The binding-energy shifts of the semiconductor and overlayer core levels upon overlayer deposition are shown

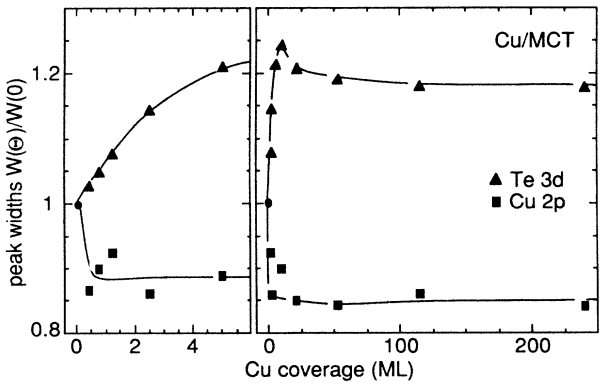

FIG. 13. Variation of the Te $3d$ and Cu $2p$ core widths with coverage for Cu/MCT.

in Fig. 14. These shifts, while clearly due to chemical interaction upon intermixing of the semiconductor and overlayer, are difficult to interpret in detail. After the initial rigid shift of 0.1 eV to higher KE due to band bending, all elements except the Hg show a gradual shift to higher BE, stabilizing at about $\Theta=21$ ML. After this coverage the intermixing is complete in the sense that the composition of the overlayer changes little with increasing Cu coverage, resulting in essentially no further changes in the core binding energies. From 0.1 to 21 ML the Cu $2p$ and Te $3d$ core levels shift 0.2—0.3 eV to higher BE, contradicting naive charge-transfer arguments that would predict the Cu and the anion to shift in opposite directions. A similar effect has been observed previously for Cr/MCT.[3] The cations also display different behavior, with the Cd shifting 0.1 eV to higher BE from the $\Theta=0.1$ ML position, while the Hg shows no shift. Given the different Pauling electronegativity values for Cd (1.7) and Hg (1.9), charge-transfer arguments would suggest that the Cd and Hg might undergo different binding energy shifts, but considering the failure of these arguments for the Cu and Te shifts, a full explanation of any of these shifts is not readily available.

D. LEED observations

The evolution of the LEED pattern with coverage for Cu/MCT differs significantly with the evolution for Cu/CdTe: Compared to the Cu/CdTe case, the Cu/MCT LEED pattern becomes much more diffuse at low coverages but ultimately remains visible at much higher coverages. More specifically, upon the initial deposition of 0.1 ML on MCT the pattern becomes much more diffuse as the Cu intermixes with the disrupts the surface. Between $\Theta=5$ and 10 ML the surface order appears to change from the initial rectangular 1×1 symmetry to a hexagonal pattern, although the extreme diffuseness of the spots does not permit definite confirmation of this change. This pattern is observed at coverages as high as 365 ML, but is finally gone at $\Theta=560$ ML. The observation of a LEED pattern at such high coverages suggests the presence in the overlayer of crystallites of a Cu-Te compound. As discussed previously, the Cu/Te ratio of the overlayer at high coverages is close to that of Cu_2Te; it should be noted that Cu_2Te has a hexagonal unit cell.[27] The disappearance of the LEED pattern at the highest coverage studied suggests that the increasing proportion of metallic Cu on the surface above 100 ML grows as disordered islands, completely covering the surface with metallic Cu by the highest coverage. Ehsani and Bené,[21] using transmission electron microscopy and diffraction, have observed for 200 Å Cu/MCT the growth of $\sim$1500 Å crystallites of Cu_2Te (with a preferred orientation direction), much larger than the Cu_2Te crystallites they observed for Cu/CdTe.

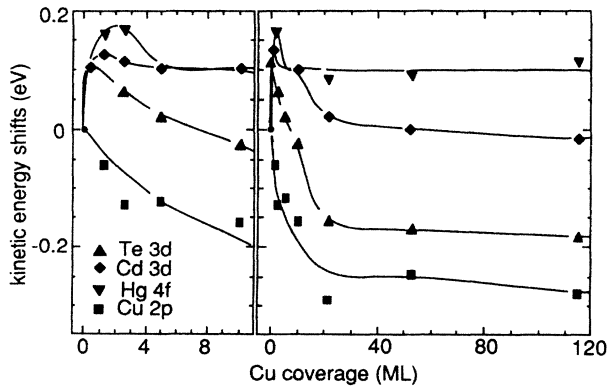

FIG. 14. Kinetic energy shifts of the semiconductor and metal core levels as a function of coverage for Cu/MCT. A positive kinetic energy shift is equivalent to a shift to lower binding energy. All energies are referenced to the Fermi level.

E. Band bending and Schottky-barrier formation

As can be seen from Figs. 9 and 14, at the initial deposition of 0.1 ML there is a rigid shift of the energy bands 0.1—0.15 eV to higher kinetic energy, signaling a downward movement relative to the VBM of the surface Fermi level from the cleaved position. Since E_F for the cleaved surface lies at the CBM (±0.1 eV) (Ref. 28) the cleaved surface is intrinsic or n type although the bulk MCT is p type. The effective Schottky barrier therefore depends on the depth of the initial n-type conversion. If the n-type region were sufficiently deep, so that the Fermi level stayed pinned to the CBM in the subsurface after the initial Cu deposition, the bands would bend 0.1 eV downwards from the subsurface providing an effective Schottky barrier to the p-type material. If on the other hand the CBM for the cleaved surface is pinned to E_F only at the surface, the shift of E_F upon Cu deposition would represent a relaxation of the Fermi level pinning 0.1 eV closer to the bulk position at the VBM. An understanding of the nature of the Fermi-level pinning for the cleaved MCT surface would be desirable, especially since virtually all metal-semiconductor work with cleaved MCT to date involves a surface which is converted n-type on cleaving.[1–6] Furthermore, electrical measurements on "thick" ($\sim$1000 Å) UHV-fabricated metal overlayers would provide a more complete understanding of the nature of the Schottky-barrier formation on MCT.

V. DISCUSSION

A. Morphology

The morphologies of the Cu/CdTe and Cu/MCT interfaces differ both in the initial formation of the interface at low coverages and in the degree and nature of the semiconductor-overlayer intermixing at high coverages. The low- and high-coverage regimes are connected since the disruption of the semiconductor surface at low overlayer coverages will affect the quantity of semiconductor anions and cations available to move into the overlayer at higher coverages.

Neither the Cu/CdTe nor the Cu/MCT interface is abrupt; for example, there is a significant concentration of Cd and Te in the overlayer in both cases. In the initial stages of interface formation, however, the MCT interface

is considerably less abrupt than the CdTe interface, with motion of Cu on the order of 10 Å or more into the semiconductor near-surface region so that no unreacted Cu is seen in the overlayer near surface below $\Theta=200$ ML; for CdTe, in contrast, unreacted Cu has started to form below 1.2-ML coverage. While for CdTe there is a depletion of Cd in approximately the first atomic semiconductor layer as Cd is pulled into the overlayer, the cation depletion for MCT is larger: The degree of surface Cd depletion for the two interfaces is similar, but for MCT by $\Theta=10$ ML there is in addition a depletion of $\sim 50\%$ of the Hg within the first ~ 20 Å of the semiconductor surface. As we shall discuss below, this is critical to the subsequent formation of the overlayer.

The instability of the Hg—Te bond[8,9] provides a natural explanation of the enhanced depletion of Hg compared to Cd, especially considering the similar small values of the heats of solution of these two elements in Cu. While the heat of formation for Cu_2Te is not significantly greater than for HgTe, the difference is sufficient in principle to account for the rebonding of Te atoms from Hg to Cu, when the depletion of Hg due to its high vapor pressure is taken into account. In addition, effects other than those considered in bulk thermodynamics may play a role in the Te rebonding. The heat of condensation of the overlayer metal on the semiconductor has been shown by Spicer *et al.*[29] to play a critical role in Schottky-barrier formation on GaAs. The heat of condensation, or clustering of overlayer atoms,[30] may also play an analogous role for Cu/MCT. Clustering or simply adsorption of the Cu overlayer atoms could provide part of the energy required to overcome the activation barrier to Te rebonding. The comparable magnitudes of the depth to which Cu moves into the MCT and the depth of Hg depletion suggest that the Hg depletion is not only a consequence of the Cu indiffusion and resulting Cu—Te bond formation at the expense of Hg—Te bonds, but also a cause of the indiffusion by permitting Cu to move relatively deep into the lattice by replacing Hg. The Cu indiffusion is also favored by the low heat of Cu-telluride formation, which permits the overlayer metal to move beneath the surface layer instead of being localized at the surface by strong reaction with Te. In contrast, for the much more reactive Al/MCT (Refs. 2 and 6) interface with $\Delta H_f(Al_2Te_3)=-76.2$ kcal/mol,[7] a correspondingly greater Hg loss is observed, equivalent to a complete loss of Hg in the first 10—15 Å by $\Theta=0.5$ ML. For this interface, in contrast to Cu/MCT, the high reactivity with Te keeps the overlayer atoms localized on the semiconductor surface while the high heat of formation still results in Hg depletion well past the surface layer.

Even for the more moderate Hg depletion in the case of Cu overlayers, unless an atom for atom replacement in the lattice occurs between Cu and Hg the depletion should result in a collapse of the lattice, enhancing Te and Cd outdiffusion into the overlayer. The effect of this intermixing enhancement manifests itself even at high coverages, as much more Te and Cd is made available for intermixing at the initial stages of interface formation than for the case of CdTe, for which only the first atomic layer or two of Te and Cd is pulled into the overlayer. Also, removal of Hg from the MCT near-surface region will result in an excess of Te at the interface which is then available for intermixing with the overlayer. This is consistent with the tentative suggestions made in Sec. III that for CdTe the amounts of Te and Cd intermixed into the overlayer may be comparable, while as discussed in Sec. IV there is 5—10 times as much Te as Cd in the Cu/MCT overlayer. Furthermore, since the small Cu-Te and Cu-Cd reactivities provides only limited inhibition[31] of either Cu indiffusion or transport of Te and Cd away from the immediate vicinity of the interface, the motion of Cu into the MCT and resulting release of Te and cations into the overlayer can continue even at very high coverages. In this case the composition of the overlayer within an XPS escape length would stabilize as soon as the initial interface formation was complete, consistent with what we observe.

B. Band bending

Band bending upon metal/CdTe interface formation has been discussed by Williams and Patterson.[12,32] They observe for a wide range of metals on cleaved CdTe a linear dependence of Schottky-barrier height upon overlayer work function in accord with the Schottky model of the barrier; this dependence has also been observed by Werthen *et al.*[33] In view of the stabilization of the Fermi-level position for Cu/CdTe by 0.1-ML coverage, at which the overlayer metal is still in a purely reacted form, the Schottky model cannot apply literally to this interface. The inappropriateness of this model for the Cu/CdTe case casts doubt upon the correctness of the model to other metal/CdTe interfaces. Williams and Patterson[12,32] and Brucker and Brillson[34] have emphasized that Cd depletion from the CdTe surface may play an important role in determining surface Fermi-level pinning positions, but thus far the exact role of the Cd vacancies has not been elucidated.

For metal/MCT interfaces, photoemission band bending data on a variety of interfaces sufficient to support examination of systematic trends is only now becoming available. For the noble metals Cu, Ag,[5] and Au,[4] upon metal deposition the Fermi level E_F moves down 0.05—0.2 eV. Deposition of the column III A overlayers Al (Refs. 2 and 6) and In (Ref. 2) moves E_F 0.4—0.8 eV upwards from its cleaved surface position near the bottom of the conduction band, resulting in a highly n-type degenerate surface after metal deposition. Finally, for the transition metals Cr,[3] Pt,[35] and Pd (Ref. 36) on MCT no band bending is observed. For none of these interfaces has the cause of the band bending or the lack thereof been unambiguously identified; many explanations have been proposed for the different interfaces. For example, motivated by the observed Hg depletion from the surface, n-type doping by Hg diffusion into the bulk has been proposed to explain the downward band bending for Al/MCT and In/MCT;[2] alternatively, doping by overlayer indiffusion has been proposed for the Al/MCT interface[6] (n-type doping) as well as for the upward band bending of the Au/MCT (Ref. 4) and Ag/MCT (Ref. 5) interfaces (p-type doping). The possibility of p-type dop-

ing by Hg vacancy formation has also been suggested for the band bending in Ag/MCT.[5] While it is quite possible that different effects dominate for the different interfaces, not all of the proposed explanations listed above give correct results for all the interfaces to which they might be expected to apply. The n-type doping by motion of Hg from the semiconductor surface into the bulk, for instance, might be expected to apply equally well to Cr/MCT as to Al/MCT, as the two interfaces show a very similar extent of Hg depletion from the surface; nonetheless the two interfaces show very different band bending. In contrast, the idea of band bending due to doping of the surface by indiffusion of the overlayer metal can be consistently applied to all the interfaces mentioned above. The noble metals are all known to be acceptors in MCT while the column III A elements Al and In are donors,[37] consistent with the band bending behavior of these elements on MCT in the overlayer doping model. Furthermore, although no data on the doping properties of Cr, Pt, or Pd appears to be available, it is very plausible that these elements, with their open-d shells and subsequent range of valences, are neutral dopants in MCT.

While Schottky-barrier (SB) formation for such semiconductors as GaAs is not generally considered to be due to overlayer doping of the semiconductor, the disruption of the semiconductor surface and motion of overlayer atoms into the semiconductor are so much greater for MCT than for, e.g., GaAs that models for SB formation on GaAs are not directly relevant to the MCT case. Thus, even if further investigation shows that SB formation for metals on MCT is not best described by an overlayer doping model, it seems likely that any mechanism for SB on MCT will differ from the mechanisms which have been suggested for GaAs.

VI. CONCLUSIONS

The difference in Hg—Te and Cd—Te bond strengths results in very different interface morphologies for Cu/MCT and Cu/CdTe. For CdTe, no significant indiffusion of the overlayer metal is seen, and a limited amount of Cd and Te diffusion into the overlayer is detected. Unreacted Cu is detected on the surface below $\Theta = 1.2$ ML. At high coverages, the Te in the overlayer is concentrated largely in a 2—8 Å thick region within a few Å of the surface of the overlayer and intermixed with Cu so that the total amount of Te in the subsurface layer is approximately equivalent to the amount of Te in 2 Å of pure Te, while the Cd in the overlayer is distributed more uniformly. For the Cu/MCT interface there is significantly more intermixing at both low and high coverages. Up to $\Theta \approx 2$—10 ML the deposited Cu migrates on the order of 20 Å into the semiconductor, displacing $\sim 50\%$ of the Hg in this region by $\Theta = 10$ ML and causing a 3—4 Å thick Cd and Hg deficient layer at the interface. For high coverages of Cu on MCT, the intermixing of Te and Cd in the overlayer is greatly enhanced compared to Cu/CdTe, so that no unreacted Cu is observed in the overlayer near-surface region until $\Theta = 200$ ML. The band bending for Cu/MCT, as well as for other metal/MCT interfaces in the literature, is consistent with doping of the semiconductor (p type for the case of Cu) by small amounts of indiffused overlayer metal.

ACKNOWLEDGMENTS

This work was supported by the Defense Advanced Research Projects Agency under Contract No. MDA-903-83-C-0108, and by gift funds from the Hughes Aircraft Company. Crystals were grown at Santa Barbara Research Center.

APPENDIX

Here we present the details of the escape depth calculation for the model presented in Sec. III D of the Te layer in the Cu overlayer for Cu/CdTe. For our model of the overlayer $c(x)$ is nonzero only for $d < x < d + \Delta$, so that

$$\frac{I_1}{I_1(0)} = K \frac{\lambda_1}{\lambda_1^S} e^{-d/\lambda_1} (1 - e^{-\Delta/\lambda_1}) \tag{A1}$$

and similarly for $I_2/I_2(0)$. Since the energy variation of photoelectron escape lengths generally has a "universal" form,[38] it is a very good approximation to take $\lambda_1/\lambda_2 = \lambda_1^S/\lambda_2^S$. Then using $R(\Theta) \equiv I_{\mathrm{Te}\ 3d}(\Theta)/I_{\mathrm{Te}\ 4d}(\Theta)$ and letting $R \equiv R(390\ \mathrm{ML})/R(0)$, we have

$$\frac{d}{\lambda_1} = (1 - A)^{-1} \left[\ln \left[\frac{1 - \exp(-\Delta/\lambda_1)}{1 - \exp(-A\Delta/\lambda_1)} \right] - \ln R \right], \tag{A2}$$

which gives the depth d of the overlayer as a function of its thickness Δ. Equation (A1), which provides a second relation between the two unknowns d and Δ, can be rewritten

$$\frac{d}{\lambda_1} = \ln(1 - e^{-\Delta/\lambda_1}) + \ln \left[K \frac{\lambda_1}{\lambda_1^S} \frac{I_1(0)}{I_1} \right]. \tag{A3}$$

A plot of d/λ_1 versus Δ/λ_1 from Eqs. (A2) and (A3) for a range of allowed values of the parameters will give a corresponding allowed range of values for d/λ_1 and Δ/λ_1.

We must now select appropriate values for the parameters. From Fig. 7 we have $R \approx 1.5$, while $I_1/I_1(0) \approx 0.2$ from Fig. 6. We shall approximate $\lambda_1 \approx 15$ Å, or $\lambda_1/\lambda_1^S = 0.8$.[39] The solution to Eqs. (A2) and (A3) does not depend strongly on these approximations. From Ref. 39, which gives experimentally determined escape lengths in CdTe, $\lambda_2^S/\lambda_1^S \approx 1.6 \approx 1/A$; more generally, the value of A will probably fall in the range $1.5 < A^{-1} < 2$, which we shall consider as the allowed range of values. Finally, the value of K, corresponding to the number density of Te atoms in the overlayer, must be specified. The lack of any chemical shift of the Te in the overlayer to higher BE than for CdTe suggests that the Cu/Te ratio in the Te-containing layer is of the same order of magnitude as for Cd/Te ratio in CdTe and not for instance an order of magnitude greater. We shall therefore take the minimum allowable Te concentration in the subsurface layer to be

equal to the Te concentration in Cu_2Te. The density of Te atoms in crystalline Cu_2Te is[29] 1.2×10^{22} Te atoms/cm^3, compared with 1.5×10^{22} Te atoms/cm^3 in CdTe, so that $K>0.8$. The concentration of Te in the layer will certainly be less than the concentration of pure Te, 2.9×10^{22}/cm^3, so that $K<2$. The resulting plot of d/λ_1 versus Δ/λ_1 for the allowed range of parameters is shown in Fig. 8.

[1]R. R. Daniels, G. Margaritondo, G. D. Davis, and N. E. Byer, Appl. Phys. Lett. **42**, 50 (1983).

[2]G. D. Davis, N. E. Byer, R. A. Riedel, and G. Margaritondo, J. Appl. Phys. **57**, 1915 (1985).

[3]D. J. Peterman and A. Franciosi, Appl. Phys. Lett. **45**, 1305 (1984); P. Philip, A. Franciosi, and D. J. Peterman, J. Vac. Sci. Technol. A 3, 1007 (1985); A. Franciosi, P. Philip, and D. J. Peterman, Phys. Rev. B **32**, 8100 (1985).

[4]G. D. Davis, W. A. Beck, N. E. Byer, R. R. Daniels, and G. Margaritondo, J. Vac. Sci. Technol. A **2**, 546 (1984).

[5]D. J. Friedman, G. P. Carey, C. K. Shih, I. Lindau, W. E. Spicer, and J. A. Wilson, Appl. Phys. Lett. **48**, 44 (1986).

[6]D. J. Friedman, G. P. Carey, C. K. Shih, I. Lindau, W. E. Spicer, and J. A. Wilson, J. Vac. Sci. Technol. A **4**, 1977 (1986).

[7]K. C. Mills, *Thermodynamic Data for Inorganic Sulphides, Selenides and Tellurides* (Butterworths, London, 1974).

[8]W. E. Spicer, J. A. Silberman, I. Lindau, A.-B. Chen, A. Sher, and J. A. Wilson, J. Vac. Sci. Technol. A **1**, 1735 (1983).

[9]A. Sher, A.-B. Chen, W. E. Spicer, and C. K. Shih, J. Vac. Sci. Technol. A 3, 105 (1985).

[10]D. J. Friedman, G. P. Carey, I. Lindau, W. E. Spicer, and J. A. Wilson, J. Vac. Sci. Technol. B **4**, 980 (1986).

[11]T. P. Humphreys, M. H. Patterson, and R. H. Williams, J. Vac. Sci. Technol. **17**, 886 (1980).

[12]M. H. Patterson and R. H. Williams, J. Cryst. Growth **59**, 281 (1982).

[13]L. J. Brillson, R. S. Bauer, R. Z. Bachrach, and J. C. McMenamin, J. Vac. Sci. Technol. **17**, 476 (1980).

[14]*Photoemission in Solids II,* edited by L. Ley and M. Cardona (Springer-Verlag, Berlin, 1978).

[15]P. Steiner and S. Hüfner, Acta Metall. **29**, 1885 (1981). This method uses a Born-Haber cycle to estimate the binding-energy shift ΔE_A (from the metallic position) for A at infinite dilution in B as $\Delta E_A=\Delta H_{sol}(A;B)-\Delta H_{sol}(A+1;B)+\Delta H_{sol}(A+1;A)$, where $\Delta H_{sol}(A;M)$ is the heat of solution of A in M, and $A+1$ represents the element with atomic number one higher than for A. We calculate the required heats of solution from the semiempirical model of Miedema *et al.* (Ref. 18). See Ref. 19 for further discussion of the application of this approach to metal/semiconductor interfaces.

[16]For example, Ref. 14, p. 315.

[17]M. G. Mason, Phys. Rev. B **27**, 748 (1983).

[18]A. R. Miedema, P. F. de Châtel, and F. R. de Boer, Physica **100B**, 1 (1980).

[19]J. Nogami, T. Kendelewicz, I. Lindau, and W. E. Spicer, Phys. Rev. B **34**, 669 (1986).

[20]M. H. Hecht and I. Lindau, J. Electron Spectrosc. Relat. Phenom. **35**, 211 (1985).

[21]H. Ehsani and R. W. Bené, J. Appl. Phys. **59**, 2808 (1986).

[22]J. A. Silberman, P. Morgen, I. Lindau, W. E. Spicer, and J. A. Wilson, J. Vac. Sci. Technol. **21**, 154 (1982).

[23]The apparent lack of Cd 4*d* attenuation in the He I spectra of Fig. 9 is deceptive: At this low kinetic energy the Cd 4*d* peaks ride on a large and nonlinear secondary electron background from the Hg 5*d* peaks, making it difficult to estimate the Cd 4*d* intensity at this photon energy. A careful inspection of Fig. 9 taking into account the background does show an attenuation of the Cd 4*d* peaks.

[24]J. J. Yeh and I. Lindau, At. Data Nucl. Data Tables **32**, 1 (1985).

[25]C. D. Wagner, W. M. Riggs, L. E. Davis, and J. F. Moulder, *Handbook of X-ray Photoelectron Spectroscopy* edited by G. E. Muilenberg (Perkin-Elmer, Eden Prairie, Minnesota, 1978), p. 22.

[26]Calculated using Ref. 18.

[27]Max Hansen, *Constitution of Binary Alloys* (McGraw-Hill, New York, 1958), p. 638.

[28]The position of the VBM was determined by a comparison with a He I spectrum taken with an angle-resolved analyzer at normal emission. For MCT at this photon energy, normal emission is much more sensitive to states near the VBM than the off-normal emission detected by the CMA. See J. A. Silberman, Ph. D. thesis. Stanford University, 1986, p. 51.

[29]W. E. Spicer, I. Lindau, P. Skeath, C. Y. Su, and P. Chye, Phys. Rev. Lett. **44**, 420 (1980).

[30]Alex Zunger, Phys. Rev. B **24**, 4372 (1981).

[31]L. J. Brillson, C. F. Bruckner, N. G. Stoffel, A. D. Katnani, and G. Margaritondo, Phys. Rev. Lett. **46**, 838 (1981).

[32]R. H. Williams and W. H. Patterson, Appl. Phys. Lett. **40**, 484 (1982).

[33]J. G. Werthen, J.-P. Häring, A. L. Fahrenbruch, and R. H. Bube, J. Appl. Phys. **54**, 5982 (1983).

[34]C. F. Brucker and L. J. Brillson, Thin Solid Films **93**, 67 (1982).

[35]D. J. Friedman, G. P. Carey, I. Lindau, and W. E. Spicer (unpublished).

[36]G. P. Carey, D. J. Friedman, I. Lindau, and W. E. Spicer (unpublished).

[37]E. S. Johnson and J. L. Schmit, J. Electron. Mater. **6**, 25 (1977).

[38]I. Lindau and W. E. Spicer, in *Synchrotron Radiation Research,* edited by H. Winick and S. Doniach (Plenum, New York, 1980).

[39]J. Szajman, R. C. G. Leckey, J. Liesegang, and J. G. Jenkin, J. Electron Spectrosc. Relat. Phenom. **20**, 323 (1980).